Int. J. Heat Mass Transfer. Vol. 31, No. 6, pp. 1137–1148, 1988
Printed in Great Britain

0017–9310/88 $3.00 + 0.00

Study of natural convection in horizontal annuli

RANGANATHAN KUMAR
Department of Mechanical Engineering, Clemson University, Clemson, SC 29631, U.S.A.

(*Received* 2 *October* 1986 *and in final form* 23 *December* 1987)

Abstract—Natural convection of gases in a horizontal annulus, where the inner cylinder is heated by the application of a constant heat flux and the outer cylinder is isothermally cooled, is studied numerically. Detailed results of temperature, velocity and heat transfer are presented for a wide range of Rayleigh numbers extending from conduction to the convection-dominated steady flow regime, and diameter ratios of 1.2–10. A crescent-shaped eddy dominates for the small diameter ratio and a kidney-shaped flow pattern appears for the large diameter ratio as observed by previous investigators in their flow visualization studies. The inner wall temperature is a function of diameter ratio and Rayleigh number. An increase in Rayleigh number based on the same temperature difference for the inner wall boundary condition of constant heat flux or constant temperature increases the heat transfer rate; however, the increase is larger for the constant heat flux case. At large diameter ratios ($\kappa \geqslant 10$), the heat transfer rates are the same for both types of heating, and a single cylinder in an infinite atmosphere gives nearly the same results.

1. INTRODUCTION

NATURAL convection in horizontal annuli has been the subject of interest for the past 25 years and many experimental, analytical and numerical papers have appeared in the literature. In most of these studies, isothermal cylinders were considered. The annulus geometry has application in solar collector receiver, thermal storage systems and transmission cables.

It is clearly established from the flow visualization study of Bishop and Carley [1] that there are two basic types of natural convection flow between horizontal cylinders; the crescent-shaped eddy pattern for small diameter ratios and the kidney-shaped eddy pattern for diameter ratios greater than 3.6. This work was extended by Powe *et al.* [2] and a chart was presented which allowed prediction of the type of unsteady flow that would occur for a wide range of cylinder combinations and annulus operating conditions. Grigull and Hauf [3] presented the results of a study similar to the one reported in ref. [1]. They observed three-dimensional flows which were not reported by ref. [1] although both investigations used the same range of variables. The conflicting results of refs. [1, 3] and Liu *et al.* [4] are discussed by Bishop *et al.* [5] who presented detailed quantitative information concerning the characteristics of a natural convective oscillatory flow between horizontal isothermal cylinders. The results of a numerical investigation obtained by Powe *et al.* [6] predicted a counter-rotating cell for small diameter ratios as seen by ref. [2] but the predicted transition to oscillatory flow was somewhat different from that given by ref. [2]. In general, the experimentally determined transition segments obtained by ref. [2] were confirmed by their numerical work [6]. Mack and Bishop [7] solved the equations for low Rayleigh numbers by using the first three terms in a power series of Rayleigh number based on inner radius. They predicted secondary cells in the top and the bottom of the annulus for very low Prandtl numbers which was later confirmed by Charrier-Mojtabi *et al.* [8]. Mahony *et al.* [9] showed numerically the effects of variable property and diameter ratio on the heat transfer and fluid flow in the horizontal annulus. Kuehn and Goldstein [10, 11] determined experimentally and numerically the heat transfer results up to a Rayleigh number of 10^5. Kuehn and Goldstein [12] also presented a correlation equation that improved upon previously published results. Different numerical schemes were utilized to solve the problem in concentric cylinders by Crawford and Lemlich [13], Projahn *et al.* [14], and Cho *et al.* [15]. The above-mentioned papers were confined to steady-state analysis of flow between horizontal isothermal cylinders.

A realistic problem of heat dissipation in transmission cables is to cool the outside surface of the cable with a coolant such as water. The inner surface has a uniform heat flux and the outer surface is isothermally cooled. The heat transfer results for this problem were determined experimentally by Van de Sande and Hamer [16] for $Ra_L > 2 \times 10^6$ for both concentric and eccentric cylinders. Constant heat flux on the inner wall was considered by Keyhani *et al.* [17] and Prasad [18] for the vertical annulus. The former reported experimental results in non-porous media and the latter obtained numerical results in porous media. Morgan [19] presented correlation equations based on the experimental data of Dyer [20] who studied heat transfer from a cylinder heated by the application of a constant heat flux in an infinite medium.

This paper presents the numerical results of steady, natural convection flow of gases between two horizontal cylinders with the inner wall maintained at constant heat flux. The cylinders are long and the flow is assumed to have axially independent properties. The flow also has vertical lines of symmetry at the top

NOMENCLATURE

c_p	specific heat at constant pressure
$\mathbf{e}_R$	unit vector in the radial direction
$\mathbf{e}_\theta$	unit vector in the tangential direction
$\mathbf{F}$	body force
g	acceleration due to gravity
$\bar{h}$	average heat transfer coefficient
k	thermal conductivity of the fluid
L	gap width, $r_o - r_i$
Nu_L	Nusselt number, $\bar{h}L/k$
p	pressure
Pr	Prandtl number, ν/α
q	constant heat flux applied on the inner wall
r	radial coordinate
R	dimensionless radial coordinate, r/L
Ra_L^*	Rayleigh number, $\beta g(qL/k)L^3/\alpha\nu$
Ra_L	Rayleigh number, $\beta g(\Delta T)L^3/\alpha\nu$
T	dimensional temperature
ΔT	temperature difference across the annulus; $(T_i - T_o)$ for isothermal heating, and $(T_{m,i} - T_o)$ for constant flux heating
u	non-dimensional radial velocity, $V'_R L/\alpha$
v, V_θ	non-dimensional tangential velocity, $V'_\theta L/\alpha$
V	velocity vector, $\mathbf{V} = V'_R\mathbf{e}_R + V'_\theta\mathbf{e}_\theta$
V'_R	dimensional radial velocity
V'_θ	dimensional tangential velocity.

Greek symbols

α	thermal diffusivity
β	coefficient of volumetric expansion
ζ	vorticity
θ	angular coordinate; measured positive clockwise from the upper vertical line of symmetry
κ	radius ratio, r_o/r_i
ξ	vector potential
ρ	density
τ	dimensionless temperature, $(T - T_o)/(qL/k)$
ψ	stream function.

Subscripts

D_i	based on inner diameter
i	inner wall
l	local quantity
L	based on gap width
m	mean value on the inner wall
max	maximum value
o	outer wall.

and the bottom of the annulus. Comparisons are made with isothermal heating. Dependence of peak and mean temperatures on the diameter ratio is addressed. The flow patterns for different diameter ratios are discussed in detail.

2. PROBLEM FORMULATION

The governing equations for a steady laminar flow with no heat generation, negligible viscous dissipation, applying the Boussinesq approximation may be written as follows:

$$\text{continuity} \quad \nabla\cdot\mathbf{V} = 0 \tag{1}$$

$$\text{momentum} \quad \rho(\mathbf{V}\cdot\nabla)\mathbf{V} = -\nabla p + \mathbf{F} - \mu\nabla\times(\nabla\times\mathbf{V}) \tag{2}$$

$$\text{energy} \quad k(\nabla\cdot\nabla)T = \rho c_p(\mathbf{V}\cdot\nabla)T \tag{3}$$

where $\mathbf{F}$ is the body force given by

$$\mathbf{F} = (-\rho g\cos\theta\,\mathbf{e}_R + \rho g\sin\theta\,\mathbf{e}_\theta). \tag{4}$$

The following equations relate velocity $\mathbf{V}$ to vorticity ζ and vector potential ξ

$$\mathbf{V} = \nabla\times\xi$$

$$\zeta = \nabla\times\mathbf{V}. \tag{5}$$

The axial component of ξ in two-dimensional flows is the stream function and henceforth will be denoted by ψ. ζ is the axial component of vorticity. The dimensionless quantities are

$$u = \frac{V'_R L}{\alpha}; \qquad v = \frac{V'_\theta L}{\alpha}$$

$$R = \frac{r}{L}; \qquad \tau = \frac{T - T_o}{(qL/k)}$$

$$Ra^* = \frac{\beta g(qL/k)L^3}{\alpha\nu}; \quad \kappa = \frac{r_o}{r_i}. \tag{6}$$

The final equations are written as

$$\frac{1}{R^2}\frac{\partial^2\psi}{\partial\theta^2} + \frac{\partial^2\psi}{\partial R^2} + \frac{1}{R}\frac{\partial\psi}{\partial R} = -\zeta \tag{7}$$

$$u\frac{\partial\zeta}{\partial R} + \frac{v}{R}\frac{\partial\zeta}{\partial\theta} = -Ra_L^* Pr\left[\frac{\partial\tau}{\partial R}\sin\theta + \frac{1}{R}\frac{\partial\tau}{\partial\theta}\cos\theta\right] + Pr\left[\frac{1}{R^2}\frac{\partial^2\zeta}{\partial\theta^2} + \frac{\partial^2\zeta}{\partial R^2} + \frac{1}{R}\frac{\partial\zeta}{\partial R}\right] \tag{8}$$

$$u\frac{\partial\tau}{\partial R} + v\frac{\partial\tau}{\partial\theta} = \frac{1}{R}\frac{\partial\tau}{\partial R} + \frac{\partial^2\tau}{\partial R^2} + \frac{1}{R^2}\frac{\partial^2\tau}{\partial\theta^2}. \tag{9}$$

In the above equations, u and v are written in terms of ψ using equations (5).

The boundary conditions on the walls are evaluated

using no slip conditions for velocity, constant heat flux on the inner wall, constant temperature on the outer wall and no cross flow in the vertical line of symmetry. The angular coordinate increases in the clockwise direction, with $\theta = 0$ at the top and $\theta = \pi$ at the bottom of the annulus. Mathematically, the boundary conditions may be stated as

$$R = \frac{r_i}{L}, \quad \frac{\partial \tau}{\partial R} = -1, \quad \psi = 0, \quad \zeta = -\frac{\partial^2 \psi}{\partial R^2}$$

$$R = \frac{r_o}{L}, \quad \tau = 0, \quad \psi = 0, \quad \zeta = -\frac{\partial^2 \psi}{\partial R^2}$$

$$\theta = 0, \pi, \quad \frac{\partial \tau}{\partial \theta} = 0, \quad \psi = 0, \quad \zeta = 0. \tag{10}$$

3. NUMERICAL PROCEDURE

The vorticity transport equation and the energy equation were solved by the false transient alternating direction implicit (ADI) method, and the stream function equation was solved by the successive over relaxation (SOR) method. Such a procedure was successfully used by Mallinson and de Vahl Davis [21] and Mahony *et al.* [9]. The specific derivation of the ADI method was a variation of the one proposed by Samarskii and Andreyev [22]. The first and second derivatives in space were approximated by central differences and the time derivatives by a first-order difference. Derivatives at the boundaries were approximated by a three-point forward or backward differencing.

A uniform $r \times \theta$ grid of 18×31 was chosen for low Rayleigh number conditions, and a semi-uniform grid of 18×31, closely spaced near the walls and the vertical boundaries, was chosen for more severe flow conditions that occurred at high Rayleigh numbers. For high diameter ratios, a 28×41 mesh was used. To check for secondary cells, a mesh size of 28×51 was used for selected cases. The solution was found to be grid independent.

The following criterion was used to check convergence at each nodal point:

$$\frac{|\phi_{new} - \phi_{old}|}{|\phi_{new}|_{max}} \leqslant \Gamma \tag{11}$$

where ϕ is the primary variable being tested, the subscripts 'old' and 'new' are the previous and present iterative values, respectively, and Γ a prespecified constant. This constant was set to 10^{-3} for the semi-uniform mesh and 10^{-4} for the uniform mesh, and was frequently lowered to 10^{-5} to maintain the energy balance to a specified tolerance.

The energy balance was maintained by checking if the average heat transfer rates on the inner and outer surfaces differed by less than 2%. The constant Γ in equation (11) was made smaller if the difference was higher than desired. The majority of the results converged to give less than 1% energy balance, and an error of up to 3% was tolerated for high Ra^*. For $\kappa = 10$, energy balance was compromised up to 5% and the convergence at each nodal point was only 10^{-3}. So, only a few results for $\kappa = 10$ appear in this paper. The number of iterations needed for convergence was dependent upon the choice of starting condition. On average, the number ranged from 100 steps to 600 steps using the computer NAS/XL60.

Validation studies have already been performed by Mahony *et al.* [9] by generating a solution that could be directly compared with previously published results. Results were compared with the experimental results of Kuehn and Goldstein [10] and several other numerical results and were found to be in excellent agreement.

4. RESULTS

Natural convection of gases in the horizontal annulus with the inner wall maintained at constant heat flux and an isothermal outer wall has been studied numerically. The results of heat transfer and fluid motion have been presented using a Boussinesq approximation for a wide range of Rayleigh numbers extending from conduction up to a point where the flow ceases to be steady, and diameter ratios of 1.2, 1.33, 1.5, 2.6, 5 and 10. Comparisons are made with the case of an isothermal inner wall for the same temperature difference based on mean inner wall temperature and outer wall temperature. The maximum inner wall temperature non-dimensionalized by the mean temperature has been obtained for various diameter ratios. The flow patterns at high Rayleigh numbers at which transition to unsteady or three-dimensional flow occurs are discussed. Thus, the objective of this paper is to find the structure of the flow and the thermal fields in the horizontal annulus obtained for a constant uniform heat flux boundary condition and their behavior with the change in diameter ratios. The numerical results for isothermal wall heating have been compared with experimental results elsewhere [9].

4.1. *Temperature field*

The temperature distribution across the annulus presented in Fig. 1 for $Ra_L^* = 3 \times 10^5$ and $\kappa = 2.6$ is similar qualitatively to the profile obtained for isothermal inner wall heating [9] for the same Ra_L and κ (comparisons of Rayleigh numbers for the two boundary conditions will be discussed later). In the plane of vertical symmetry, where there is no angular velocity, the temperature continues to decrease slowly in the core along the radial direction until the outer boundary layer is reached where the temperature falls off sharply once again. At 45°, a temperature inversion appears in the middle of the annulus. The cold fluid moving upward gets recirculated to the outer core while slightly warming up. Such an inversion is also seen at other angular positions. The fluid in the bot-

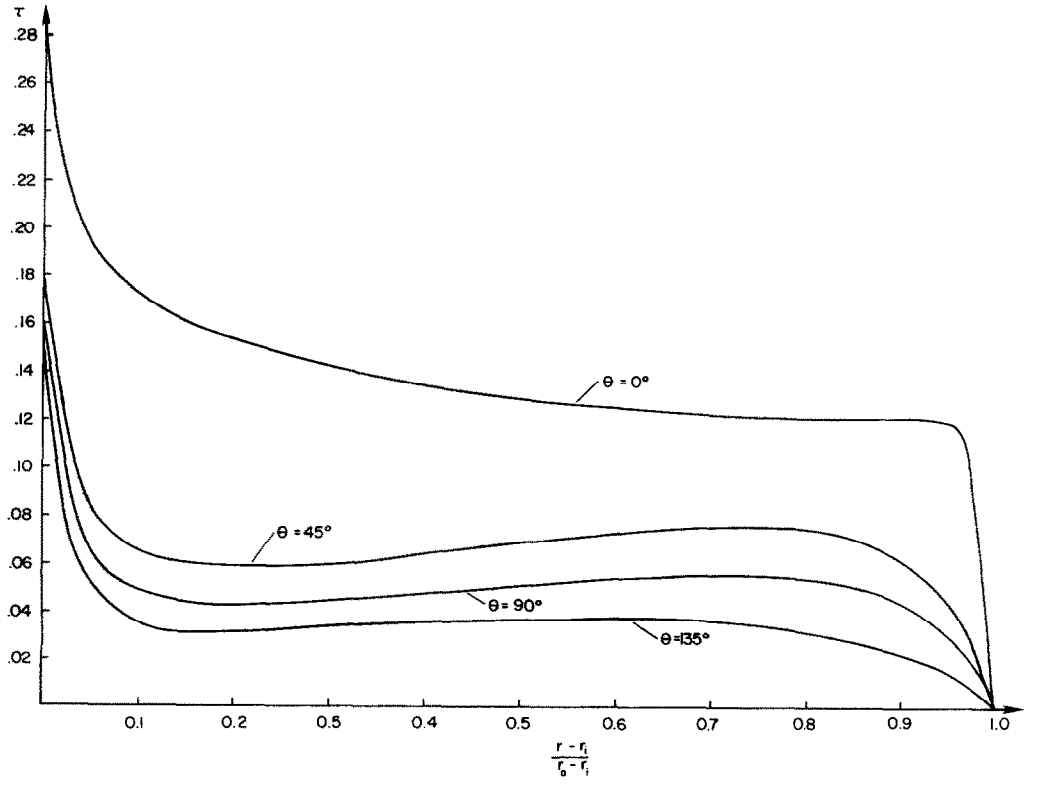

FIG. 1. Non-dimensional temperature profiles for $\kappa = 2.6$ and $Ra_L^* = 3 \times 10^5$. Angular positions are marked on the profiles.

Table 1. Normalized temperature at $R = 0.1$

	$\frac{\tau_{0.1}}{\tau_i}$							
	$Ra_L^* = 1 \times 10^5$				$Ra_L^* = 5 \times 10^5$			
$\frac{D_o}{D_i}$	0°	45°	90°	135	0°	45°	90°	135°
1.2	0.89	0.82	0.75	0.7				
1.33					0.83	0.72	0.66	0.55
1.5	0.85	0.76	0.70	0.65				
2.6	0.80	0.65	0.57	0.52	0.75	0.54	0.47	0.38
5.0	0.74	0.56	0.46	0.41	0.68	0.41	0.30	0.25

tom portion of the annulus is relatively stagnant and stays colder. In both cases of constant heat flux and isothermal heating there is a drop in temperature within a short distance from the inner cylinder at all θ-locations. However, this drop in temperature is sharper for the uniform heat flux condition producing a much thinner boundary layer. Hence, the effective sink temperature occurs closer to the inner wall, that is, at about $(r-r_i)/(r_o-r_i) = 0.1$ rather than 0.25 as in isothermal heating. Table 1 lists the percentage drop in temperature at one-tenth the annular width at four angular locations. As κ is increased to 5, for $Ra_L^* = 10^5$, the sink temperature at $(r-r_i)/(r_o-r_i) = 0.1$ falls to 74% of the maximum temperature, and the drop in temperature is sharper reaching 56% at $\theta = 45°$. The fluid temperature at $(r-r_i)/(r_o-r_i) = 0.1$ continues to decrease along θ to 41% of the maximum temperature at 135°. Thus, the stratification is seen to be strong in the upper part of the annulus at high diameter ratios and Rayleigh numbers. As the diameter ratio is decreased, there is relatively more activity in the bottom part of the annulus and hence the temperature decreases to only 70% of the wall value even at 135° for $\kappa = 1.2$. For a given gap width, the Rayleigh number is increased by increasing the heat flux on the inner wall. Hence, as the Rayleigh number increases, the temperature gradient increases, resulting in a sharper drop in temperature occurring closer to the inner wall for the same diameter ratio as is evident from Table 1.

The peak and mean temperatures on the uniform heat flux wall are useful quantities in engineering applications. The maximum temperature always occurs at the top of the inner cylinder, as can be expected, for all Rayleigh numbers and diameter ratios (Fig. 2). The temperature decreases steadily along the inner wall to the bottom line of symmetry. For a diameter ratio of 1.2, at $\theta = 180°$, the temperature decreases to approximately 40% of the maximum temperature. However, as the diameter ratio is increased, the temperature profile appears to be much smoother and flatter. In each of the profiles, an inflexion point develops. The slope, $\partial\tau_i/\partial\theta$ is also seen to decrease at 2° and the inflexion point moves away

from the top line of symmetry as the diameter ratio increases, and the profile levels off earlier midway between the top and the bottom of the inner wall. Thus, the inner wall temperature is seen to be strongly dependent on diameter ratio. As diameter ratios are further increased, the temperatures are expected to be nearly uniform on the inner wall as in isothermal heating. Thus, the heat transfer rates will be nearly the same for both isothermal and uniform heat flux boundary conditions at high diameter ratios for a given Rayleigh number.

The ratio of the maximum to the mean temperatures on the inner wall given in Table 2 confirms the arguments given above. As pointed out earlier, the mean temperature approaches the maximum value as the diameter ratio increases; however, this approach is faster for lower Rayleigh numbers. That is, when the diameter ratio is large for low Rayleigh numbers, due to low velocities, the temperature on a large portion of the inner wall remains constant. For all diameter ratios, the maximum temperature on the inner wall stays below twice its mean temperature.

4.2. *Heat transfer results*

If a mean temperature $T_{m,i}$ is determined on the inner wall, the heat transfer coefficient is given by

$$\bar{h}(T_{m,i} - T_o) = q \tag{12}$$

from which the average Nusselt number can be defined as

Table 2. Normalized maximum temperature

D_o/D_i		Ra_L^* 10^4	5×10^4	10^5	5×10^5
5.0		1.392	1.494	1.540	1.652
2.6	$\tau_{max}/\tau_{m,i}$	1.395	1.500	1.552	1.681
1.5		1.628	1.658	1.671	—
1.33		1.664	1.697	1.711	1.744
1.20		1.805	1.858	1.881	—

$$Nu_L = \frac{1}{\tau_m} \tag{13}$$

where τ_m is the non-dimensionalized mean temperature. The heat transfer results are presented in terms of Nu_L vs Ra_L^* in Fig. 3 for various diameter ratios. At very low Rayleigh numbers, the heat transfer rate is due to conduction and the numerical results are predicted to within 1% of the theoretical values of the conduction heat transfer rate

$$Nu_L = \frac{\kappa - 1}{\ln \kappa}. \tag{14}$$

As the diameter ratio increases from 1.2 to 10, the flow regime is seen to extend. Beyond the conduction regime, as the Rayleigh number increases, the heat transfer rate increases for all diameter ratios. This is consistent with the non-dimensional inner mean temperature becoming smaller as the diameter ratio gets larger, as discussed in the previous section. Since τ is defined as $\tau = (T - T_o)/(qL/k)$, as the heat flux is increased, Rayleigh number and dimensional temperature increase; however, the rate of increase of heat flux is larger than that of the dimensional temperature that τ decreases with Rayleigh number. The rate of increase of Nu_L with Ra_L^* depends slightly on the diameter ratio. At high diameter ratios, the rate of increase is slower. Since the curves beyond the pseudo-conduction region are straight lines on log–log coordinates, Nu_L for each diameter ratio may be represented by an equation of the form $Nu_L = C\,Ra_L^{*n}$. The values of C and n are dependent on the diameter ratio and are given in Table 3. As the diameter ratio is increased, the heat transfer rate must approach that for a horizontal cylinder in an infinite atmosphere. Based on the experimental data of Dyer [20] on laminar free convection on a cylinder with uniform heat flux in an infinite atmosphere, Morgan [19] recommended a correlation

$$Nu_{D_i} = 0.55 Ra_{D_i}^{0.233}. \tag{15}$$

Although the range of Rayleigh numbers used by

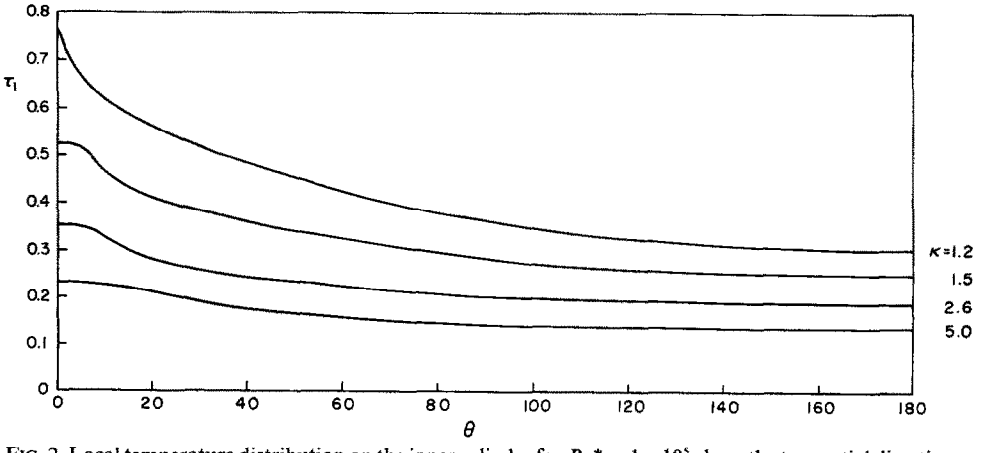

FIG. 2. Local temperature distribution on the inner cylinder for $Ra_L^* = 1 \times 10^5$ along the tangential direction.

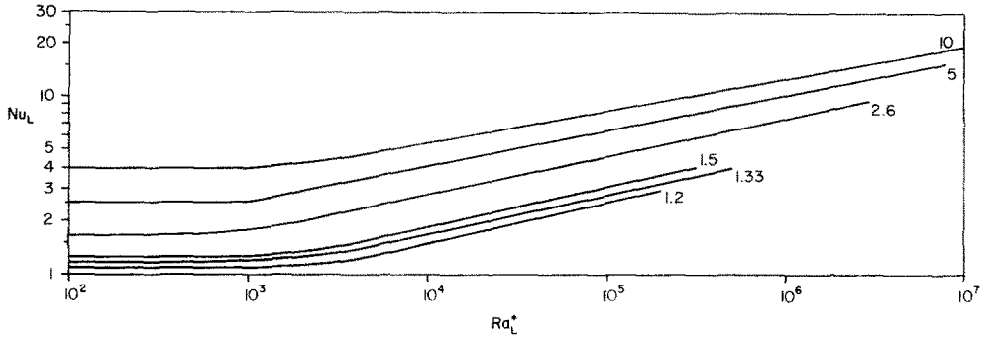

FIG. 3. Heat transfer results for different diameter ratios.

Table 3. $Nu_L = C\,Ra_L^{*n}$

κ	C	n
1.2	0.194	0.222
1.33	0.213	0.222
1.5	0.240	0.222
2.6	0.374	0.217
5.0	0.640	0.200
10.0	0.921	0.189

Dyer [20] was beyond the range presented in this paper, the extension of the present numerical results for $\kappa = 10$ predicted the heat transfer rate within 8% of Morgan's [19] correlation at $Ra_L \simeq 2 \times 10^4$. Thus, beyond $\kappa = 10$, the single cylinder results may be used to predict the heat transfer rate reasonably well. This fact is also substantiated by the plot of Nu_L vs κ in Fig. 4. Two observations can be made here. One is that for different Ra_L^*, the curves are not linear, and hence any kind of heat transfer correlation cannot include a constant exponent of diameter ratio; rather, the exponent of Ra_L^* should be a function of κ. Secondly, the heat transfer rate reaches an asymptotic value beyond a certain diameter ratio. At $Ra_L^* = 10^6$, the curves appear to become flatter earlier. Such a trend is also seen in Fig. 3 where Nu_L vs Ra_L^* curves come closer together for different κ's at high Ra_L^*. It seems reasonable to conclude that for $\kappa = 15$, the annulus results may be replaced by single cylinder results without loss of accuracy.

The local heat flux on the cold wall is given by

$$\frac{q_i}{q} = -\left.\frac{\partial \tau}{\partial R}\right|_{r=r_i}. \tag{16}$$

This dimensionless heat flux on the outer cylinder is given for $Ra_L^* = 10^5$ and 5×10^5 in Fig. 5. A high percentage of heat is rejected at the top of the outer cylinder. As the radius ratio is decreased for the same Ra_L^*, the percentage of heat rejected close to the top line of symmetry increases. The local heat flux is also seen to increase with Rayleigh number.

4.3. *Comparison of isothermal and heat flux boundary conditions*

In order to effectively compare the heat transfer results of constant heat flux and isothermal boundary

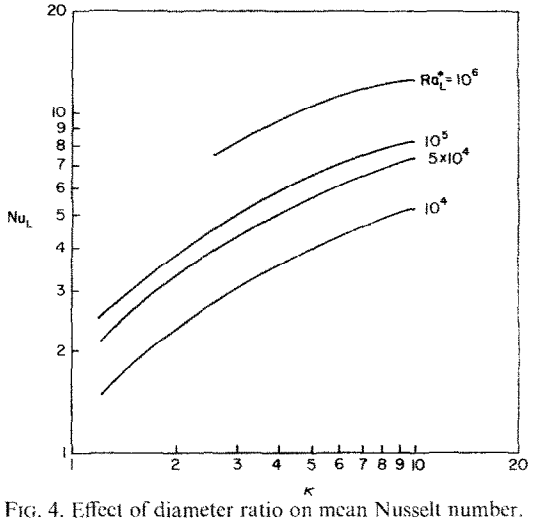

FIG. 4. Effect of diameter ratio on mean Nusselt number.

conditions, realizing that the two cases are distinct, one could speak in terms of similar conditions (same Ra, κ, etc.) if

$$T_i - T_o = T_{m,i} - T_o \tag{17}$$

where $(T_i - T_o)$ is the applied temperature difference for the isothermal case and $T_{m,i}$ is the mean temperature on the inner wall in the uniform heat flux case. The Rayleigh number, Ra_L, for the above condition may be easily derived to yield

$$Ra_L = \frac{Ra_L^*}{\overline{Nu}_L}. \tag{18}$$

It must be emphasized that such a comparison is possible only if the temperature difference and hence the Rayleigh number in both cases are identical. Some interesting results emerge in the heat transfer rate for both cases as shown in Fig. 6. The Nusselt numbers are equal in both cases in the conduction flow regime. However, it is also seen that the flow regime gets slightly extended for all the diameter ratios in the heat flux case. Beyond the pseudo-conduction region, an increase in Ra_L increases the heat transfer rates for both types of heating, but the rate of increase is larger for the constant heat flux case. This is not surprising since the temperature gradient was already seen to be

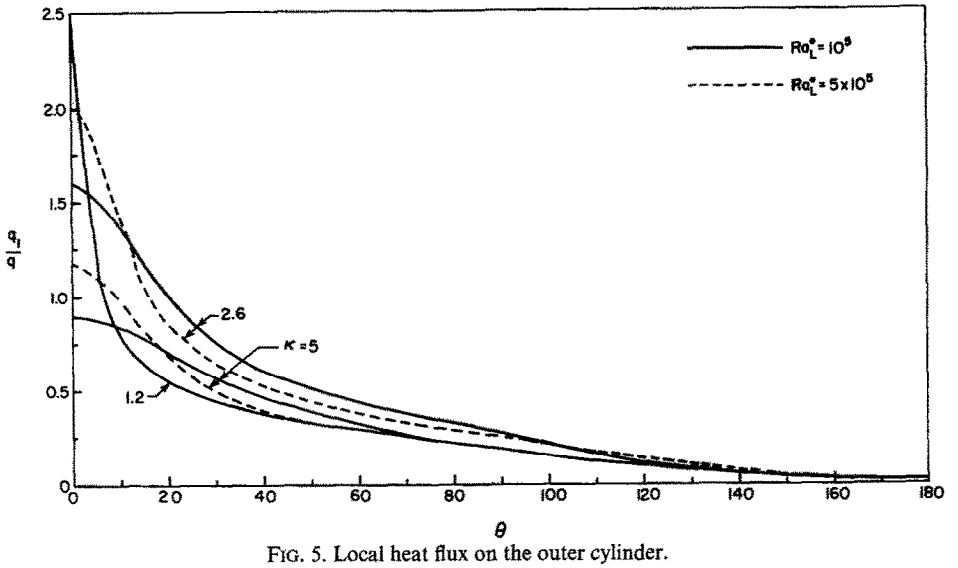

FIG. 5. Local heat flux on the outer cylinder.

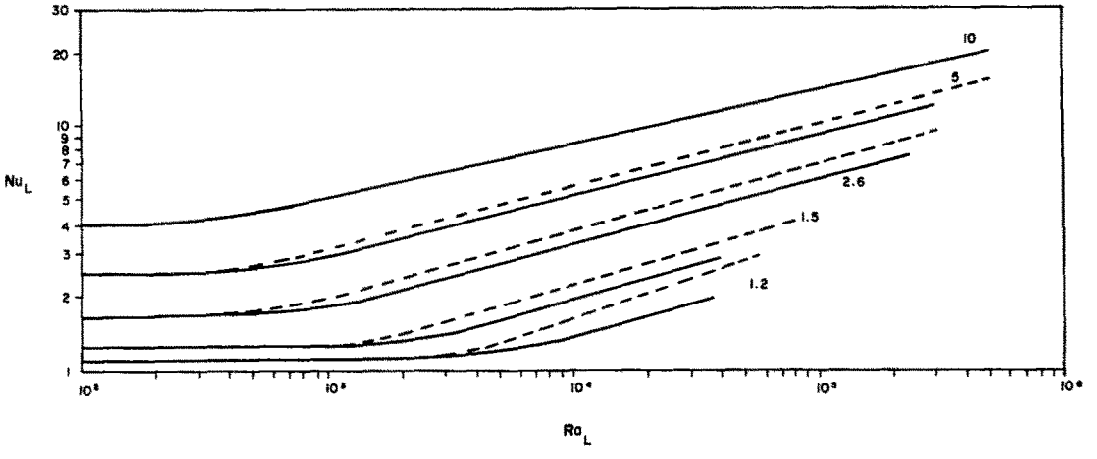

FIG. 6. Comparison of heat transfer results for heat flux boundary condition (------) and isothermal boundary condition (———).

much higher for the constant heat flux boundary condition compared to isothermal heating. This behavior is prominent for small κ's for example, for $\kappa = 1.2$, Nu_L at 10^4 is 19% larger for the constant heat flux case, but increases to 30% compared to the isothermal case at 3×10^4. At $Ra_L = 10^4$, the percentage difference in heat transfer drops from 19 to 10% when κ is increased from 1.2 to 5. However, the increase in heat transfer rate for the constant heat flux condition diminishes as the diameter ratio increases until $\kappa = 10$ is reached when both types of heating show minor changes in heat transfer results.

For $\kappa \geqslant 10$, the heat transfer rates will be the same for both types of heating, given by a single equation $Nu_L = C\,Ra_L^{*n}$, provided $\Delta T = T_{m,i} - T_o$. Morgan's [19] correlations of experimental data for a horizontal cylinder in an infinite medium for the two types of heating based on the consideration $\Delta T = T_{m,i} - T_o$ in the range $10^5 < Ra_{D_i} < 4\times10^6$ are

$$Nu_{D_i} = 0.55 Ra_{D_i}^{0.233} \quad \text{(heat flux)} \tag{19a}$$

$$Nu_{D_i} = 0.48 Ra_{D_i}^{0.25} \quad \text{(isothermal)}. \tag{19b}$$

The present numerical results for $\kappa = 10$ in the range covering the onset of motion to nearly $Ra_L \simeq 2\times10^4$ yield

$$Nu_{D_i} = 0.622 Ra_{D_i}^{0.228}. \tag{20}$$

Although constant C has a different value compared to the correlation given in equations (19), the exponent 'n' attains a nearly constant value throughout the laminar regime for both constant heat flux and isothermal boundary conditions for high diameter ratios. At $Ra_{D_i} = 20\,000$, the numerical results predict the results given by equations (19) within 8%. The percentage difference decreases at high Ra_{D_i} (10^5–4×10^6) at which Dyer's [20] data were obtained.

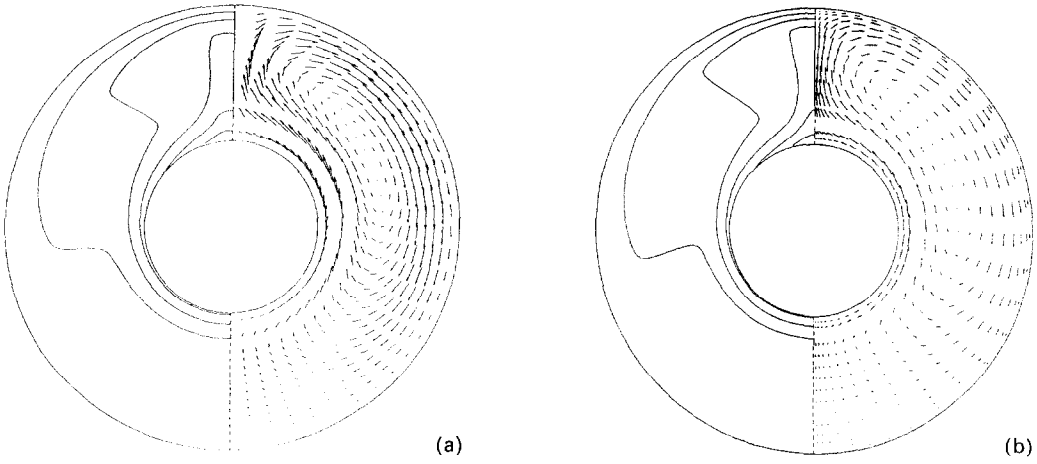

FIG. 7. Isotherms (left) and velocity vectors (right) for $\kappa = 2.6$: (a) $Ra_L^* = 6 \times 10^4$; (b) $Ra_L^* = 1 \times 10^5$.

4.4. *Flow field*

Isotherms and velocity vectors are presented in Fig. 7(a) for a representative case of $\kappa = 2.6$ and $Ra_L^* = 6 \times 10^4$. For clarity, a few points are omitted in the computational domain for plotting purposes. The bottom region is essentially stagnant with low velocities with the isotherms forming concentric circular patterns. However, in the top half of the cylinder, the fluid is recirculated making the outer layer warmer. The transport of hot fluid to the outer cylinder is also depicted by the isotherms. As the Rayleigh number increases to 1×10^5 (Fig. 7(b)), the velocities increase, the center of rotation moves toward the line of vertical symmetry but stays in the middle of the gap width. The isotherms exhibit an inversion, and the streamlines are crescent-shaped eddies as observed by Bishop and Carley [1]. A clearer picture of the flow emerges as the dimensionless tangential velocity is plotted across the annular width in Fig. 8 for $\kappa = 2.6$ and different Rayleigh numbers. For low Ra_L^*, consistent with the low temperature gradient near the inner cylinder, the velocity values are lower. As Ra_L^* increases from 6×10^4 to 3×10^5, the velocity gradient increases near the inner and outer cylinders, but the upward and downward flow are still balanced equally about the center of the gap width. As Ra_L^* is further increased to 7×10^5, at $(r-r_i)/(r_o-r_i) > 0.1$, the velocity tends to be small, and is predominantly upward until $(r-r_i)/(r_o-r_i) = 0.7$. This is because the center of rotation has moved higher up towards the vertical line of symmetry. The flow behavior at $Ra_L^* = 3 \times 10^6$ will be discussed later.

The tangential velocity profiles for the heat flux and isothermal heating in Figs. 9(a) and (b) at $Ra_L = 5 \times 10^4$ once again reveal the large velocity gradient close to the inner wall for the heat flux case due to the large temperature gradient. In both cases, the velocity attains a peak at 45°, and the profiles are similar at all angles, in the upper half of the annulus, in general. Although it is not appropriate to compare the actual velocities for the two cases at different positions in the annular width, the ratio of velocities may be considered for comparison of the two cases. At 135°, the peak velocity is only half the peak velocity at 90° for isothermal heating whereas it is two-thirds for the heat flux case. The profile at 135° also seems to be more symmetric about the center of the gap width for the present case. Between $0.2 < (r-r_i)/(r_o-r_i) < 0.8$, the velocities at all angles are nearly the same in Fig. 9(a). Thus, the flow is seen to be more active in the bottom portion of the annulus for a uniform heat flux inner boundary for the same annulus conditions.

It is confirmed by Bishop and Carley [1], Powe *et al.* [2, 6] that a secondary cell forms near the top of the annulus for small diameter ratios. Multiple cells were seen to occur for $D_i/L \geqslant 8$. In order to trace secondary cells in the present numerical work, a finer grid of 28×51 $(r \times \theta)$ was chosen. The appearance of the secondary cell for $\kappa = 1.2$ at $Ra_L^* = 5 \times 10^5$ was monitored by a change in value of the stream function. This value was too small and could appear only as a faint line as shown by Powe *et al.* [6] in their numerical study. The objective of this work is not to predict the transition segments for the heat flux boundary condition, and such an experiment was undertaken mainly to validate our numerical results. As Torrance [23] pointed out, the truncation error inherent in any numerical study would lead to spurious instabilities. However, in light of the excellent agreement of our numerical results [9] with the experimental data of ref. [10], no spurious instability is seen to have contributed to any erroneous flow pattern. A series of vector plots are presented in Figs. 10(a)–(f) for Rayleigh numbers near but slightly below transition, and $\kappa = 1.5$, 2.6 and 5.0.

The Rayleigh numbers above which the numerical results failed to converge are given in Table 4. Since the equations are written for a two-dimensional steady flow with a vertical line of symmetry, it is very difficult to judge whether the flow will become oscillatory or three-dimensional beyond a certain Rayleigh number given in Table 4 for a given inverse gap width, D_i/L. However, some interesting flow patterns are obtained,

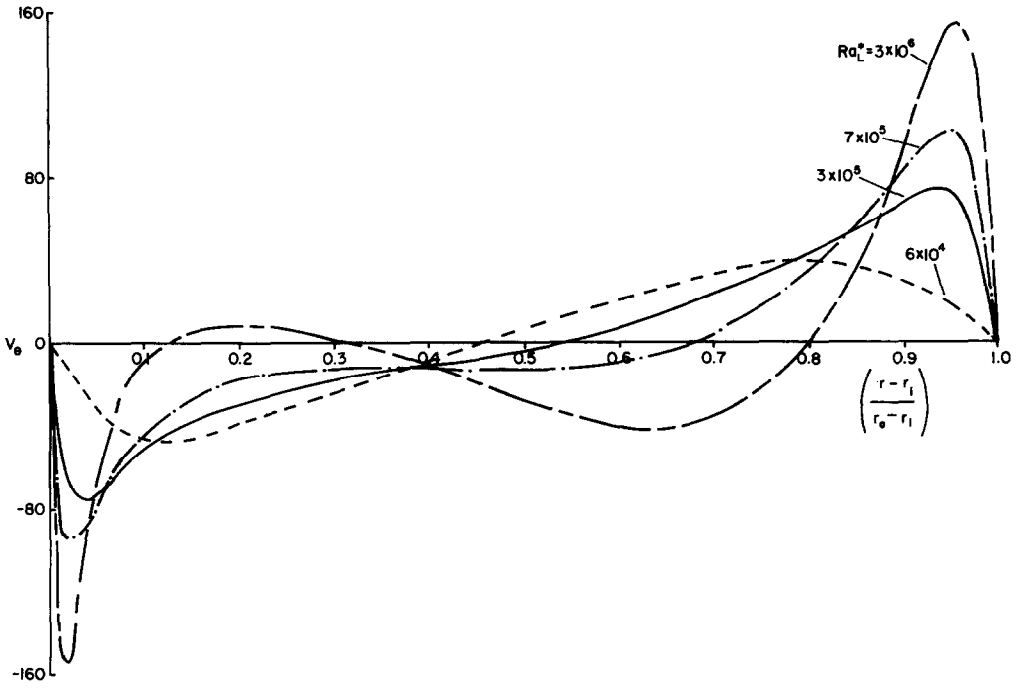

FIG. 8. Non-dimensional tangential velocity profiles for $\kappa = 2.6$ at $\theta = 90°$. Ra_L^* are marked on the profiles.

some of which were seen in photographic studies earlier [1] for isothermal cylinders.

The crescent-shaped eddy pattern is seen in Fig. 10(a) just below transition for $D_i/L = 4$. It stays crescent throughout the steady flow regime and the center of rotation does not move up high enough in order to provide room for secondary cells that probably will emerge at higher Ra_L^*. The flow behaved similarly for all $\kappa \leqslant 1.8$. Powe *et al.* [6] in their numerical work concentrated on multiple cells and hence they limited their study to $\kappa < 1.72$. Above this diameter ratio, as shown in Fig. 10(d), for $\kappa = 2.6$, the center of rotation moves closer to the line of symmetry. Nearly two-thirds of the annular width is occupied by slow upflow and the flow is strong and downward close to the outer cylinder. As the Rayleigh number is increased from 5×10^5 to 3×10^6, following Figs. 7(b), 10(c) and (d), the center of rotation approaches the outer cylinder while moving towards the line of symmetry. At $Ra_L^* = 3 \times 10^6$ (Fig. 10(d)), in the region around $\theta = 90°$, the flow turns towards the inner cylinder, and the flow is upward and downward alternately along the radial line as seen in the tangential velocity plot of Fig. 8 for the same Rayleigh number. The effect of higher diameter ratio on the flow pattern is seen in Figs. 10(e) and (f). Once again, the center of rotation moves up and towards the outer cylinder as Ra_L^* is increased. But, the crescent-shaped eddy transforms into a clear kidney-shaped pattern in Fig. 10(d) for $\kappa = 2.6$, as seen in the photographic studies of Bishop and Carley [1] between isothermal cylinders for $\kappa = 3.67$. Adjacent to the kidney-shaped eddy, the flow bends towards the inner cylinder before moving upward again as in $\kappa = 2.6$. Comparing Figs. 10(d) and (f) at high Ra_L^*, there is a larger body of relatively stagnant fluid at the bottom of the annulus as κ increases from 2.6 to 5.0.

Table 4. Critical Rayleigh number

D_o/D_i	D_i/L	Ra_L^*†
5	0.5	1.3×10^7
2.6	1.25	3×10^6
1.5	4	3.1×10^5
1.33	6	5×10^5
1.2	10	2×10^5

† Rayleigh number beyond which the solution did not converge.

5. CONCLUSIONS

This paper reports the numerical results obtained for a natural convective flow of gases between two horizontal cylinders, with the inner wall maintained at constant heat flux and an isothermal outer wall. The heat transfer and fluid flow results are presented for diameter ratios of 1.2, 1.33, 1.5, 2.6, 5.0 and 10 and $100 \leqslant Ra_L^* \leqslant 10^7$. Wherever possible, results were compared with the results obtained for flow between two isothermal cylinders, when the temperature differences in both cases were the same. Based on the heat transfer, temperature and velocity profiles and velocity vector plots, the following conclusions may be made.

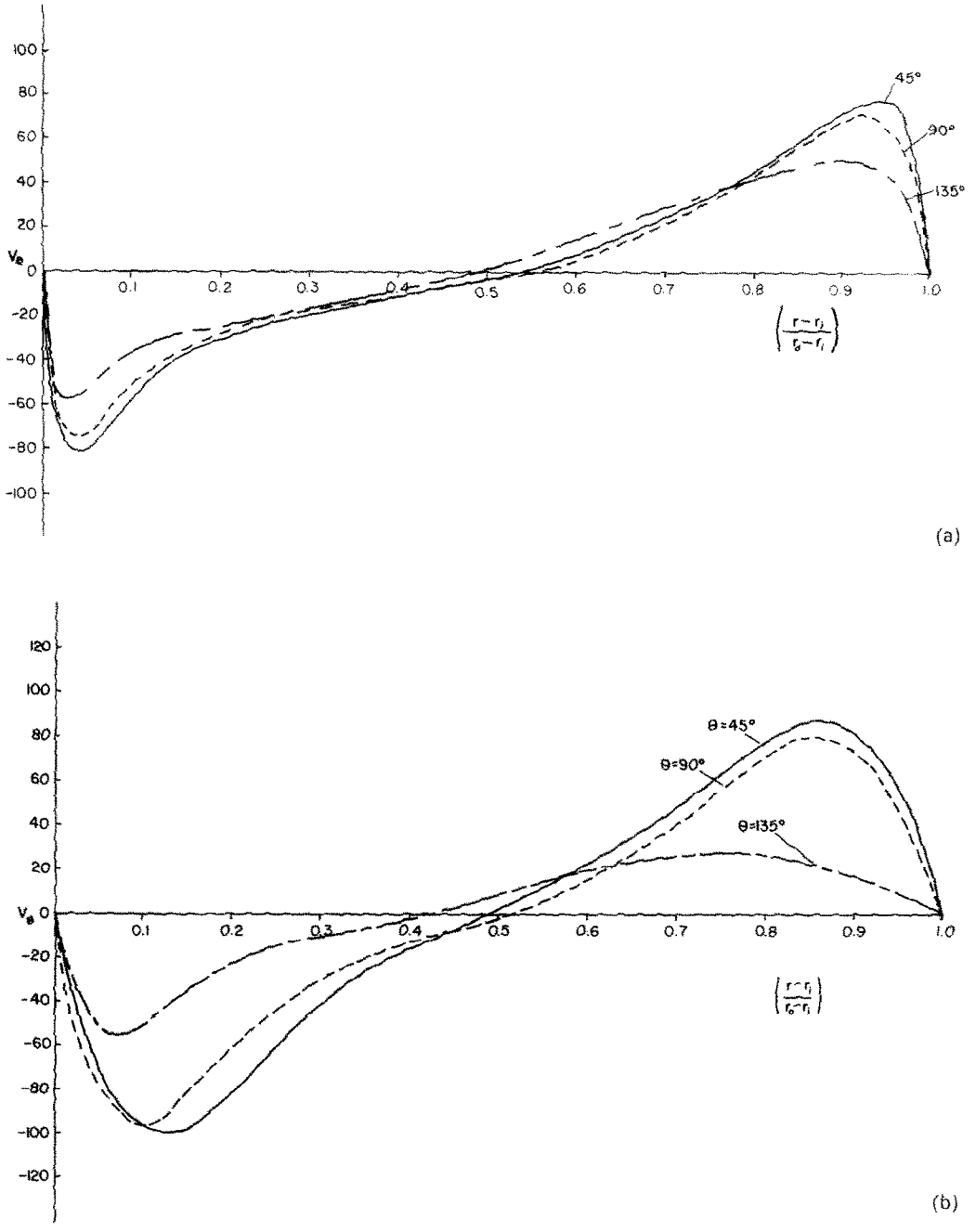

FIG. 9. Comparison of non-dimensional tangential velocity profiles for $\kappa = 2.6$ at $Ra_L = 5 \times 10^4$: (a) constant heat flux boundary conditions; (b) constant temperature boundary condition.

(1) The constant heat flux on the inner cylinder results in a lower effective sink temperature compared with isothermal heating.

(2) The inner wall temperature is strongly dependent on the diameter ratio. The ratio of peak temperature to the mean temperature increases with Rayleigh number but has the opposite effect on diameter ratio. Also, as the diameter ratio increases, for the same Rayleigh number, the effective sink temperature becomes smaller.

(3) In the convection-dominated region, Nu_L can be represented by an equation of the form $Nu_L = C\,Ra_L^{*n}$. The values of C and n are the diameter ratio.

(4) For a diameter ratio of 10, the heat transfer results predicted Morgan's [19] correlation for a single cylinder with a uniform heat flux boundary condition within 8% for $Ra_{D_i} = 2 \times 10^4$, showing that for large diameter ratios, free cylinder heat transfer coefficients are approached monotonically.

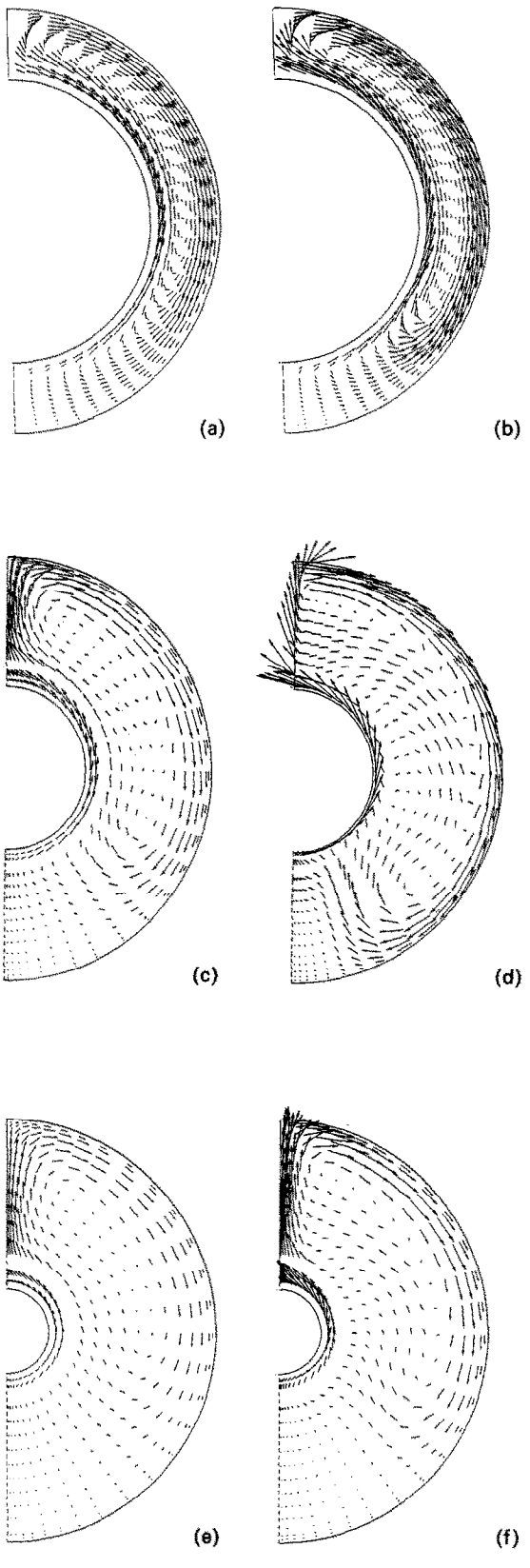

FIG. 10. Velocity vectors: (a) $\kappa = 1.5$, $Ra_L^* = 1 \times 10^5$; (b) $\kappa = 1.5$, $Ra_L^* = 3 \times 10^5$; (c) $\kappa = 2.6$, $Ra_L^* = 5 \times 10^5$; (d) $\kappa = 2.6$, $Ra_L^* = 3 \times 10^6$; (e) $\kappa = 5.0$, $Ra_L^* = 5 \times 10^6$; (f) $\kappa = 5$, $Ra_L^* = 3 \times 10^6$.

(5) Heat transfer rate is higher for the constant heat flux case than isothermal heating when the temperature difference is the same in both cases. The percentage difference in heat transfer diminishes with increase in diameter ratio.

(6) Most of the heat is rejected within 20° from the top line of symmetry on the outer cylinder for small diameter ratios. The heat rejection becomes more uniform around the outer cylinder as the diameter ratio increases.

(7) A crescent-shaped eddy dominates the flow in the case of small diameter ratios. For a diameter ratio of 5, a kidney-shaped pattern forms as observed between isothermal cylinders by Bishop and Carley [1] who performed a flow visualization study between isothermal cylinders at $\kappa = 3.67$. The flow is faster near the outer cylinder and more active in the bottom portion of the annulus compared to isothermal heating at the same Rayleigh number. At high Rayleigh numbers, as the diameter ratio is increased, there is more stagnant fluid at the bottom with the inception of a kidney-shaped flow pattern.

REFERENCES

1. E. H. Bishop and C. T. Carley, Photographic studies of natural convection between concentric cylinders, *Proc. Heat Transfer Fluid Mech. Inst.* 63–78 (1966).
2. R. E. Powe, C. T. Carley and E. H. Bishop, Free convective flow patterns in cylindrical annuli, *J. Heat Transfer* **91,** 310–314 (1969).
3. U. Grigull and W. Hauf, Natural convection in horizontal cylindrical annuli, *Proc. Third Int. Heat Transfer Conf.*, Paper No. 60, Vol. 2, pp. 182–195 (1966).
4. C. Y. Liu, W. K. Mueller and F. Landis, Natural convection heat transfer in long horizontal cylindrical annuli, *Int. Dev. Heat Transfer*, Paper No. 117, Part V, pp. 976–984 (1961).
5. E. H. Bishop, C. T. Carley and R. E. Powe, Natural convective oscillatory flow in cylindrical annuli, *Int. J. Heat Mass Transfer* **11,** 1741–1752 (1968).
6. R. E. Powe, C. T. Carley and S. L. Carruth, A numerical solution for natural convection in cylindrical annuli, *J. Heat Transfer* **92,** 210–220 (1971).
7. L. R. Mack and E. H. Bishop, Natural convection between horizontal concentric cylinders for low Rayleigh numbers, *Q. J. Mech. Appl. Math.* **21,** 223–241 (1968).
8. M. C. Charrier-Mojtabi, A. Mojtabi and J. P. Caltagirone, Numerical solution of a flow due to natural convection in horizontal cylindrical annulus, *J. Heat Transfer* **101,** 171–173 (1979).
9. D. N. Mahony, R. Kumar and E. H. Bishop, Numerical investigation of variable property effects on laminar natural convection of gases between two horizontal isothermal concentric cylinders, *ASME J. Heat Transfer* **108,** 783–789 (1986).
10. T. H. Kuehn and R. J. Goldstein, An experimental and theoretical study of natural convection in the annulus between horizontal concentric cylinders, *J. Fluid Mech.* **74,** 695–719 (1976).
11. T. H. Kuehn and R. J. Goldstein, A parametric study of Prandtl number and diameter ratio effects on natural convection heat transfer in horizontal cylindrical annuli, *J. Heat Transfer* **102,** 768–770 (1980).
12. T. H. Kuehn and R. J. Goldstein, Correlating equations for natural convection heat transfer between horizontal

circular cylinders, *Int. J. Heat Mass Transfer* **19**, 1127–1134 (1976).
13. L. Crawford and R. Lemlich, Natural convection in horizontal concentric cylindrical annuli, *I.E.C. Fund.* **1**, 260–264 (1962).
14. V. Projahn, H. Reiger and H. Beer, Numerical analysis of laminar convection between concentric and eccentric cylinders, *Numer. Heat Transfer* **4**, 131–146 (1981).
15. C. H. Cho, K. S. Chang and K. H. Park, Numerical simulation of natural convection in concentric and eccentric horizontal cylindrical annuli, *J. Heat Transfer* **104**, 624–630 (1982).
16. E. Van de Sande and B. J. G. Hamer, Steady and transient natural convection in enclosures between horizontal circular cylinders (constant heat flux), *Int. J. Heat Mass Transfer* **22**, 361–370 (1979).
17. M. Keyhani, F. A. Kulacki and R. N. Christensen, Free convection in a vertical annulus with constant heat flux on the inner wall, *J. Heat Transfer* **105**, 454–459 (1983).
18. V. Prasad, Numerical study of natural convection in a vertical porous annulus with constant heat flux on the inner wall, *Int. J. Heat Mass Transfer* **29**, 841–854 (1986).
19. V. T. Morgan, The overall convective heat transfer from smooth circular cylinders. In *Advances in Heat Transfer* (Edited by T. F. Irvine and J. P. Hartnett), Vol. 11, pp. 199–265. Academic Press, New York (1975).
20. J. R. Dyer, Laminar natural convection from a horizontal cylinder with a uniform convective heat flux, *Trans. Inst. Engng, Aust.* **MC1**, 125–128 (1965).
21. G. D. Mallinson and G. de Vahl Davis, The method of false transient for the solution of coupled elliptic equations, *J. Computational Phys.* **12**, 435–461 (1973).
22. A. A. Samarskii and V. B. Andreyev, On a high-accuracy difference scheme for an elliptic equation with several space variables, *USSR Comp. Math. Math. Phys.* **3**, 1373–1382 (1963).
23. K. E. Torrance, Comparison of finite difference computations of natural convection, *J. Res. Natl Bur. Stand.* **72B**, 281–301 (1968).

ETUDE DE LA CONVECTION NATURELLE DANS UN ESPACE ANNULAIRE HORIZONTAL

Résumé—On étudie numériquement la convection naturelle des gaz dans un espace annulaire horizontal dont le cylindre intérieur est chauffé par un flux constant et le cylindre externe refroidi isothermiquement. On présente des résultats détaillés sur la température, la vitesse et le transfert de chaleur, pour un large domaine du nombre de Rayleigh allant depuis la conduction jusqu'au régime de convection et pour des rapports de diamètre de 1,2 à 10. Un tourbillon de forme croissante domine pour un petit rapport de diamètre, et une configuration d'écoulement en rognon apparait pour un grand rapport, comme observé par des chercheurs antérieurs dans leurs travaux de visualisation. La température de la paroi intérieure est une fonction du rapport de diamètre et du nombre de Rayleigh. Une croissance du nombre de Rayleigh basé sur la même différence de température, pour la condition de flux de chaleur constant ou de température uniforme sur le cylindre intérieur, augmente le transfert thermique; néanmoins, l'accroissement est plus grand pour le cas du flux de chaleur constant. Aux grands rapports de diamètre ($\kappa \geqslant 10$), les taux de transfert thermique sont les mêmes pour les deux types de chauffage et un cylindre unique dans une atmosphère infinie donne à peu près les mêmes résultats.

UNTERSUCHUNG DER NATÜRLICHEN KONVEKTION IN WAAGERECHTEN RINGRÄUMEN

Zusammenfassung—Die natürliche Konvektion von Gasen in einem waagerechten Ringraum, bei dem der innere Zylinder mit einem konstanten Wärmestrom beheizt und der äußere Zylinder bei konstanter Temperatur gekühlt wird, wird numerisch untersucht. Detaillierte Ergebnisse bezüglich Temperatur, Geschwindigkeit und Wärmeübergang werden über einen weiten Bereich der Rayleigh-Zahl dargestellt, vom Gebiet der reinen Wärmeleitung bis hin zur stationären Konvektionsströmung. Das Durchmesserverhältnis beträgt zwischen 1,2 und 10. Bei kleinen Durchmesserverhältnissen treten vor allem halbmondförmige Wirbel auf, während bei großen Durchmesserverhältnissen nierenförmige Strömungsformen auftreten, wie sie auch von anderen Autoren durch Sichtbarmachen der Strömung beobachtet wurden. Die Temperatur des Innenrohres hängt vom Durchmesserverhältnis und von der Rayleigh-Zahl ab. Eine Erhöhung der Rayleigh-Zahl, die auf dieselbe Temperaturdifferenz bezogen ist, erhöht den Wärmeübergang sowohl für die innere Randbedingung konstanter Temperatur als auch bei konstanter Wärmestromdichte, bei letzterem Fall ist die Verbesserung allerdings größer. Bei größeren Durchmesserverhältnissen ($\kappa \geqslant 10$) ist der Wärmeübergang bei beiden Randbedingungen gleich und erreicht fast den Wert eines einzelnen Zylinders im unendlichen Raum.

ИССЛЕДОВАНИЕ ЕСТЕСТВЕННОЙ КОНВЕКЦИИ В ГОРИЗОНТАЛЬНЫХ КОЛЬЦЕВЫХ КАНАЛАХ

Аннотация—Численно изучается естественная конвекция газов в горизонтальных кольцевых каналах, внутренний цилиндр которых нагревается постоянным тепловым потоком, а внешний—изотермически охлаждается. Представлены подробные данные о температуре, скорости и теплопереносе для широкого диапазона чисел Рэлея, охватывающего режимы устойчивых кондуктивных и конвективных течений, и отношения диаметров от 1,2 до 10. По данным визуализации течения, полученным ранее другими авторами, в случае малых значений отношения диаметров, преобладает серповидный вихрь, в то время как при больших значениях возникает картина течения, напоминающая по форме фасоль. Внутренняя температура стенки является функцией отношения диаметров и числа Рэлея. Увеличение числа Рэлея, основанное на одной и той же разности температур для граничного условия для внутренней стенки с постоянным тепловым потоком или постоянной температурой, интенсифицирует теплоперенос, причем интенсификация сильнее при постоянном тепловом потоке. При больших отношениях диаметров ($\kappa \geq 10$), теплообмен одинаков для обоих типов нагрева, а случай единичного цилиндра в бесконечной среде дает почти такие же результаты.